Broadband mm-Wave Propagation Characterization of Planar Groove Gap Waveguide

Titus Oyedokun*[1], Riana H. Geschke[2,1] and Tinus Stander[3]

[1] Department of Electrical Engineering, University of Cape Town. South Africa.
[2]Fraunhofer Institute for High Frequency Physics and Radar Techniques FHR. Wachtberg, Germany.
[3]Carl and Emily Fuchs Institute for Microelectronics, Department of Electrical, Electronic and Computer Engineering, University of Pretoria. South Africa.
*Correspondence: Titus Oyedokun, Department of Electrical Engineering, University of Cape Town. South Africa. oydtit001@myuct.ac.za

Abstract. We present, experimental broadband propagation characterization of a planar groove gap waveguide (PGGWG) from 29 to 40 GHz. The transmission line Q-factor is found to vary from 110 to 130 over the band, which is shown by comparison of measurement data to be comparable to substrate integrated waveguide (SIW). PGGWG is found to have a phase constant of nearly double that of SIW using the same materials and manufacturing process. This is a significant result for system miniaturization.

Keywords: Groove gap waveguide, planar waveguide, substrate integrated waveguide.

1 INTRODUCTION

The next generation of mm-wave communication networks will require frequency agile planar filters with low loss.[1] Substrate integrated waveguide (SIW) filters are often used, but since frequency agility requires DC isolated terminals for varactor biasing, [2] typically multiple etched annular rings and bridging wires[3, 4] are required for bias routing. The requirement of DC isolation would also complicate the integration of frequency agility with existing slow-wave modifications[5,6,7]to SIW, as these all require a solid via row sidewall and, consequently, would introduce a galvanic connection between the upper and lower conducting planes.

A recently proposed planar groove gap waveguide (PGGWG) structure,[8] a planar implementation of the micro-machined groove gap waveguide (GGWG), [9, 10] provides a propagation medium similar to SIW but with the benefit of DC isolated planes, which is advantageous in the biasing of active devices.[11] The basic operating principles of PGGWG have been described previously, [8, 11] and are similar to that of GGWG.[9, 10]

Previous analyses of PGGWG's properties have been based on resonant structures, where cavity Q-factor is used as a metric.[8] In this paper, we present new results on the broadband propagation characteristics of the medium in a manner similar to what was

presented for machined GGW previously.[10] This work extends on our previous analyses[8, 11] by presenting a broadband back-to-back experimental comparison between PGGWG and SIW, highlighting the slow-wave property of PGGWG.

2 GEOMETRY AND OPERATION PRINCIPLE

PGGWG is realized within a parallel plate waveguide by using blind vias and catch pads to create an electromagnetic bandgap (EBG) medium on either side of a groove[8] (Figure 1). The waveguide sidewall is replaced by an artificial magnetic conductor (AMC). Here, three rows of blind vias are placed on either side of a groove, w, between the top and bottom conducting planes. The EBG unit cell consists of a round catch pad of diameter p_d, connected to the top conducting plane with a via of diameter v_d. The substrate height h is chosen to be less than, or equal to, $\lambda_g/4$ at the bandgap center. This is necessary for the suppression of parallel plate mode propagation. The substrate thickness h_a between the top of the EBG cell and the bottom conducting plane is also less than $\lambda_g/4$. All layers, including the prepreg in the stack-up, have the same relative permittivity.

The EBG unit cell stopband can be controlled by varying the geometric parameters (h, v_d and p_d) of the unit cell. This can be observed from the variation in magnitude of S_{21}, as well as the dispersion diagrams, as shown in Figures 2, 3 and 4.

The variation of the bandgap with increase via height h, as observed in Figure 2, results in a shift of the bandgap to lower frequencies. This is as a result of reduced effective capacitance between the bottom conducting plane and the round catchpad. A change in the bandgap as the via diameter v_d increases can also be observed in Figure 3. This is due to increased unit cell inductance. In Figure 4, it is shown that as the surface area of the catch pad p_d increases, the capacitive load between the EBG surface and the top conducting plate changes, resulting in a shift in the bandgap. It is, therefore, possible to control the bandgap whilst restricting h and h_a to available laminate thicknesses. The pitch p is chosen to be the minimum value which still allows for a manufacturable gap between successive catch pads of diameter p_d.

The groove within the rows of the EBG vias creates a propagation channel similar to that in a rectangular waveguide, [8] leading to transmission characteristics to which the theoretical analysis of GGWG[10] may be applied. The TE_{10} E-fields can be observed within the groove in Figure 5. The groove width w is chosen to ensure that the fundamental TE_{10} mode, similar to that obtained in SIW, propagates within the stopband of the parallel plate modes[8]. Figure 5 further shows that the field is contained within the inner two rows of EBG cells. It is, therefore, expected that increasing the number of EBG cell rows beyond 3 will not affect the characteristics of the line, while decreasing it to 2 or less would lead to increased insertion loss.

3 EXPERIMENTAL DESIGN

The PGGWG build stack-up as shown in Figure 1 is realized with a sequential build process. The EBG via holes are drilled through a single layer substrate core thickness of h. These via holes are then electroplated with a 17 micron copper thickness, t. Thereafter, the catch pad is etched on top of the vias as annular rings. This is followed by laminating a layer of prepreg of thickness h_a. Finally, a 17 micron copper cladding is deposited onto the top of the prepreg surface for the plate of the PGGWG.

The dimensions of the PGGWG waveguide, as shown in Figure 1, are w = 5.48 mm, h = 0.508 mm, h_a = 0.106 mm, v_d = 0.3 mm, p_d = 0.7 mm, p = 0.95 mm. MercuryWave 9350 substrate with ε_r = 3.5 is used for both laminate layers. A coplanar waveguide (CPW) transition excites the fundamental TE_{10} mode within the groove of the PGGWG, which in turn is connected to 1.85 mm end-launch connectors. This can be seen in Figure 6(a) of the fabricated PGGWG circuits. Figure 7 shows the sectional cut X-X` in Figure 6(a) across the AMC side wall, indicating manufacturing errors of 14 µm (2.8%) in h, 36 µm (5.1%) in p_d and 32 µm (30%) in h_a. The error in h_a impacts on the resonant frequency of the unit cell. An increase in gap height h_a, decreases the capacitance between the catchpad and the top conducting plate. As a result, the parallel plate suppression band is reduced.

For comparison, an SIW transmission line is designed to have the TE_{10} mode cutoff at 28 GHz (Figure 6(b)). The SIW line is a_{siw} = 3.4 mm wide, and delineated by vias of diameter v_{dsiw} = 0.3 mm at a pitch p_{siw} = 0.45 mm. The implementation uses the same substrate material as PGGWG with the same multi-layer stack-up of total height h_{siw} = 0.618 mm. Thru-Reflect-Line (TRL) calibration standards were manufactured for both PGGWG and SIW, to de-embed the additional loss introduced by the transitions and the connectors.

4 MEASUREMENT RESULTS

The attenuation constant, α, and phase constant, β, are extracted from S-parameter simulation and measurements of 7 mm lengths of PGGWG and SIW transmission line. The extracted attenuation constants are shown in Figure 8, indicating that PGGWG features marginally higher attenuation than SIW. The variation in PGGWG attenuation above 36 GHz is due to the breakdown of the EBG stopband condition. Similar results were noted previously in other EBG-based planar transmission media.[12]

The phase constant of ≈ 1100 rad/m midband in Figure 9 is significantly higher than that of SIW and the phase velocity a factor 1.57 slower (Figure 10). These results confirm previous observations[8] that PGGWG resonators are smaller than SIW resonators at the same resonant frequency, which may be exploited for system miniaturization. The deviation at 38 GHz is due to the breakdown of the EBG stopband, leading to erratic transmission behaviour. The remaining discrepancies between the

simulated and measured phase constant for PGGWG may be attributed to the manufacturing errors shown in Figure 7 and discussed in Section 3.

The transmission line Q-factors, [13] defined as

$$QTL = \frac{\beta}{2\alpha}$$

are plotted in Figure 11. It is found that the mid-band values of ≈ 120 are comparable between PGGWG and SIW. The high peak in PGGWG line Q-factor observed at 39 GHz is due to the near-zero attenuation constant observed in Figure 8, which in turn is an artifact of imperfect de-embedding of the transitions.

5 CONCLUSION

This paper presents, for the first time, the broadband propagation characteristics of PGGWG at Ka-band in a direct comparison to SIW. It is found that the structure exhibits comparable Q-factor, but much higher phase constant than SIW, which allows the miniaturization of components on PGGWG as compared to SIW. We have therefore demonstrated the benefit of size reduction of transmission lines implemented on PGGWG as compared to SIW.

6 ACKNOWLEDGMENTS

The use of CST Microwave Studio and NI AWR Microwave Office academic licenses are acknowledged. This work is supported in part by the National Research Foundation of South Africa (Scholarship 99870 and Grant number 88100).

References

1. Bozzi M, Georgiadis A, Wu K. Review of substrate-integrated waveguide circuits and antennas. *IET Microwaves, Antennas & Propagation* 2011;5(8):909
2. Eccleston K. Mode analysis of the corrugated substrate integrated waveguide. *IEEE Transactions on Microwave Theory and Techniques*, 2012;60(10):3004-3012.
3. Sirci S, Martinez J, Taroncher M, Boria V. Analog tuning of compact varactor-loaded combline filters in substrate integrated waveguide. *Proceeding of European Microwave Conference*, 2012;257-260.
4. Sirci S, Martinez JD, Taroncher M, Boria VE. Varactor-loaded continuously tunable SIW resonator for reconfigurable filter design. *Proceeding of European Microwave Conference*, 2011; 436-439.
5. He Y, Li Y, Zhu L, Bagci H, Erricolo D, Chen P. Waveguide dispersion tailoring by using Embedded Impedance Surfaces. *Physical Review Applied, 2018; 10:044024.*
6. Hrabar S, Bartolic J, Sipus Z. Waveguide miniaturization using uniaxial negative permeability metamaterial," *in IEEE Transactions on Antennas and Propagation, 2005;53(1):110-119.*
7. Niembro-Martín A et al. Slow-Wave substrate integrated waveguide. *IEEE Transactions on Microwave Theory and Techniques, 2014;62(8):1625-1633.*
8. Oyedokun T, Geschke R, Stander T. Experimental characterisation of planar groove gap waveguide and cavity. *Proceeding of European Microwave Conference*, 2017;436-439.
9. Rajo-Iglesias E, Kildal PS. Groove gap waveguide: A rectangular waveguide between contactless metal plates enabled by parallel-plate cut-off. *Proceeding of European Conference on Antennas and Propagation, 2010;* 1-4.
10. Berenguer A, Fusco V, Zelenchuk D, Sanchez-Escuderos D, Baquero-Escudero M, Boria-Esbert V. Propagation characteristics of groove gap waveguide below and above cutoff. *IEEE Transactions on Microwave Theory and Techniques*, 2016; 64(1):27-36.
11. Oyedokun T, Geschke R and Stander T. A Geometric study of tunable planar groove gap waveguide cavities. *IOP Conference Series: Materials Science and Engineering*, 2018; 321:012008.
12. Sánchez J, Bachiller C, Esteban H, Belenguer, Nova V, Boria V. New decoupled empty substrate integrated waveguide realisation. *Electronics Letters*, 2017;53(17):1203-1205.
13. Somlo, P. Some Aspects of the measurement of the Q factor of transmission lines. *IEEE Transactions on Microwave Theory and Techniques*, 1963;11(6):472-478.

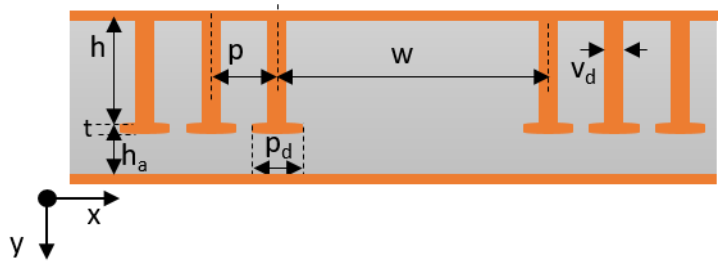

Figure 1. Cross-section of the PGGWG geometry

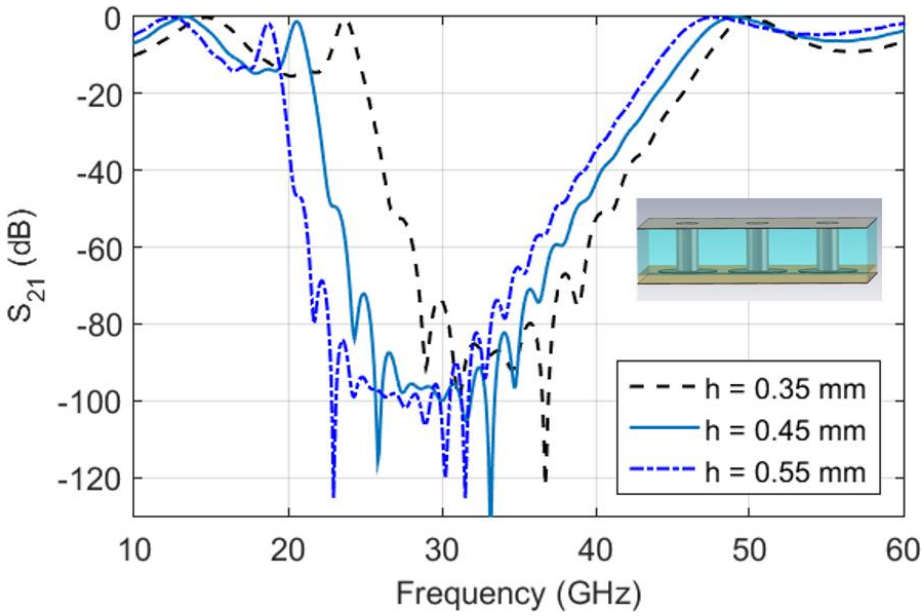

Figure 2. Magnitude of S_{21}(dB) and dispersion diagram for varying via height h of the EBG unit cells with the following dimensions: h_a = 0.106 mm, v_d = 0.3 mm, p_d =0.8 mm, p = 0.95 mm, ε_r = 3.5, tan δ = 0.004. (A) Magnitude of S_{21} (dB) for varying via height h of the EBG unit cells.

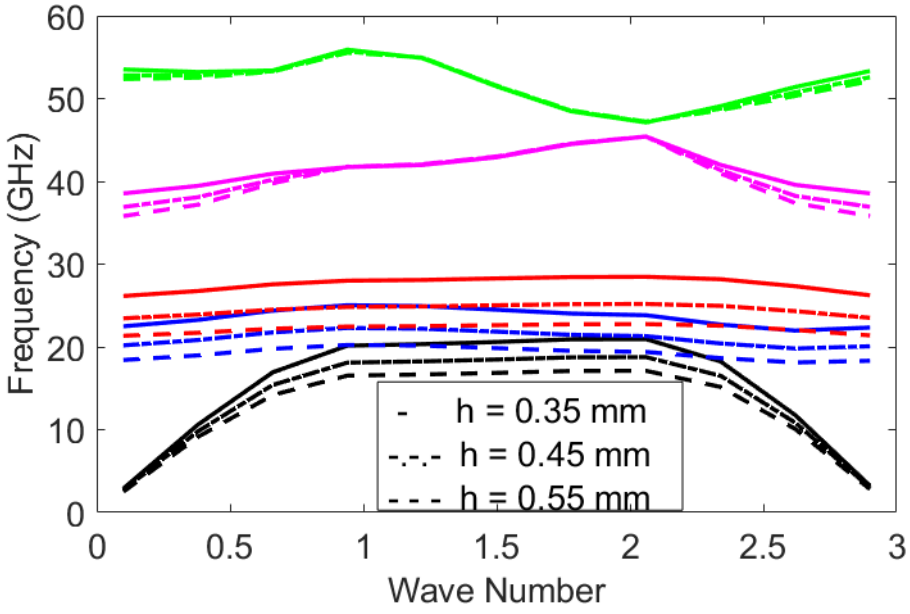

Figure 2b. Dispersion diagram for varying via height h of the EBG unit cells

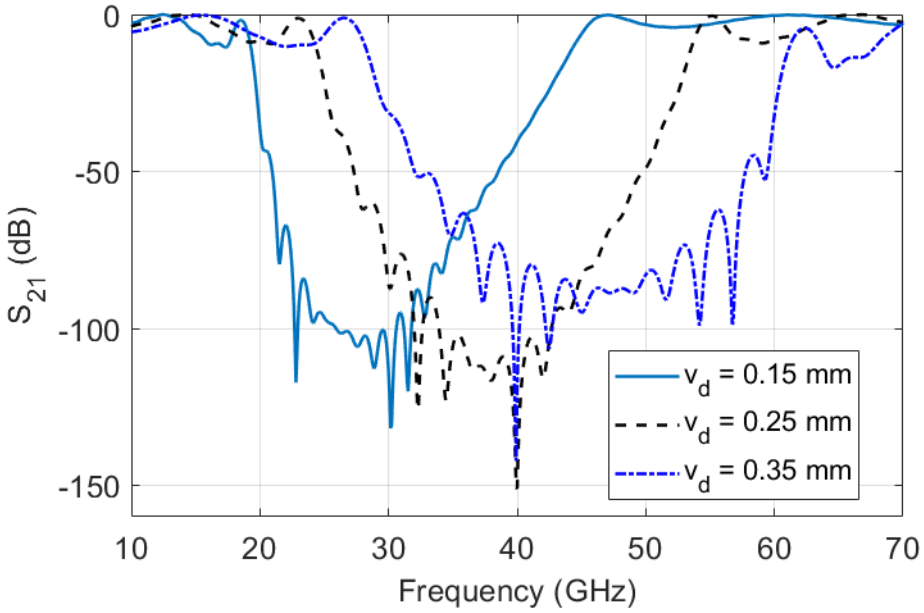

Figure 3a. Magnitude of S_{21}(dB) and dispersion diagram for varying via diameter, v_d of the EBG unit cells with the following dimensions: h_a = 0.106 mm, h = 0.508 mm, p_d =0.8 mm, p = 0.95 mm, ε_r = 3.5, tan δ = 0.004.. (A). Magnitude of S_{21}(dB) for varying via diameter, v_d of the EBG unit cells

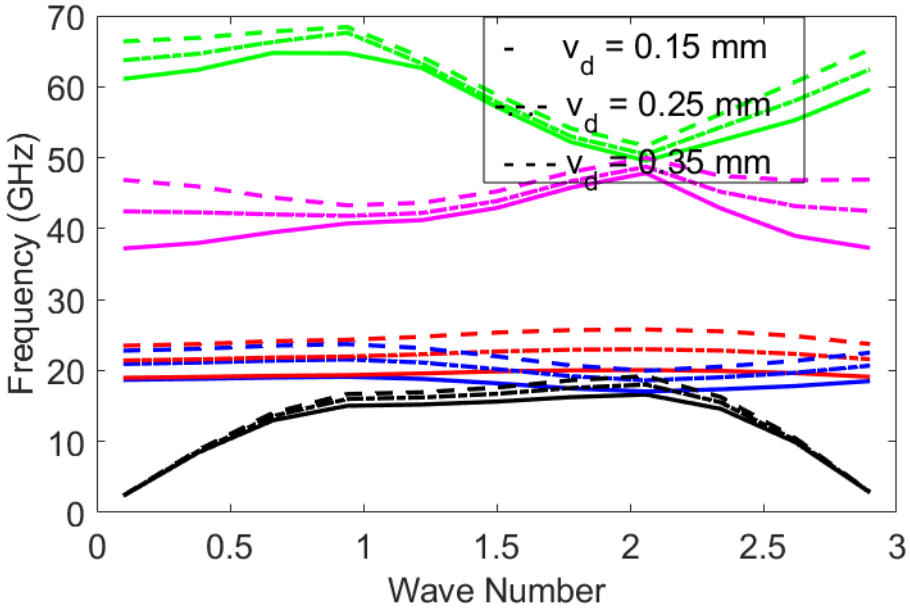

Figure 3b. Dispersion diagram for varying via diameter, v_d of the EBG unit cells

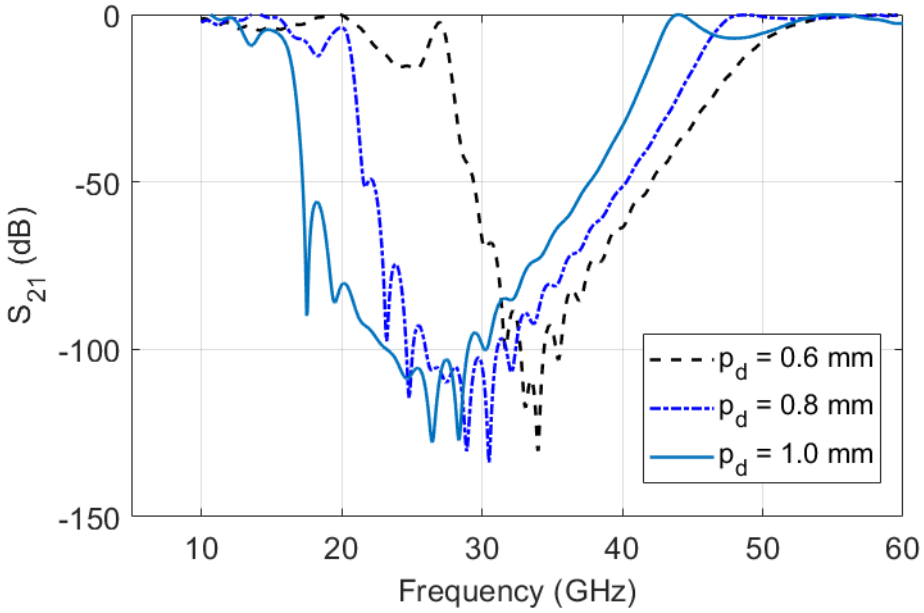

Figure 4 Magnitude of S_{21}(dB) and dispersion diagram for varying catch pad diameter, p_d of the EBG unit cells with the following dimensions: h_a = 0.106 mm, h = 0.508 mm, p = 0.95 mm, ε_r = 3.5, tan δ = 0.004. (A) Magnitude of S_{21}(dB) for varying catch pad diameter, p_d of the EBG unit cells.

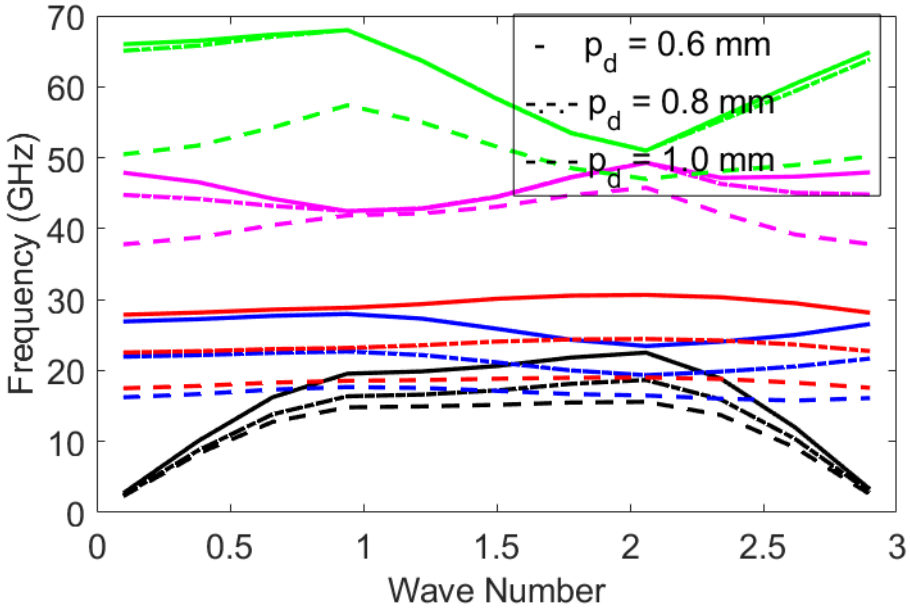

Figure 4b. Dispersion diagram for varying catch pad diameter, p_d of the EBG unit cells.

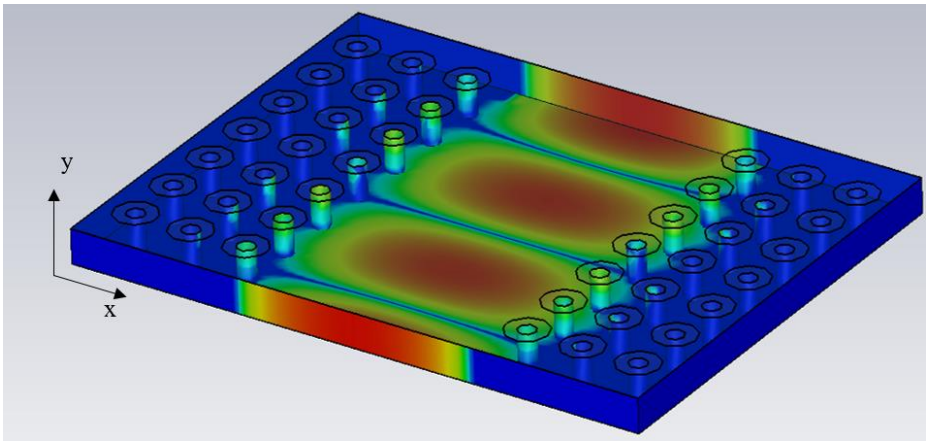

Figure 5. 3D view of the PGGWG in CST Microwave Studio 2016, with E-field magnitude superimposed

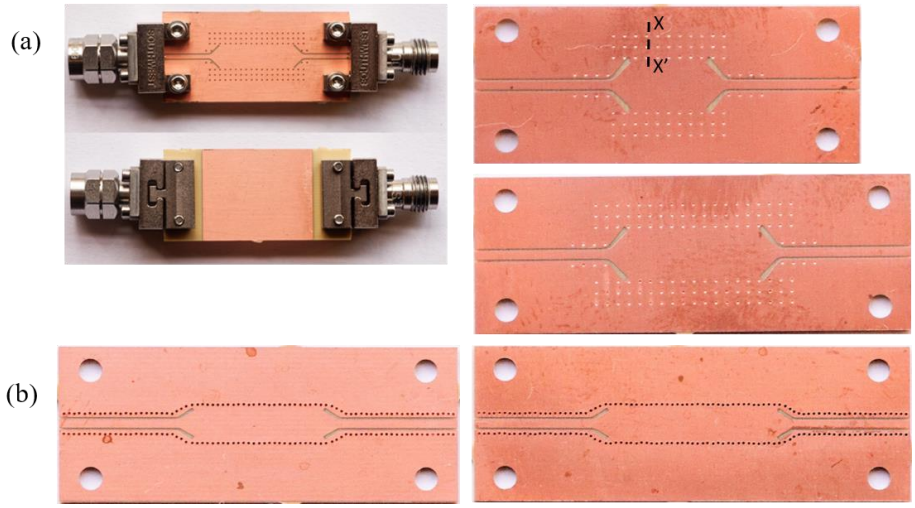

Figure 6. Photographs of the fabricated circuits with two line lengths. (a) PGGWG circuits. (b) SIW circuits.

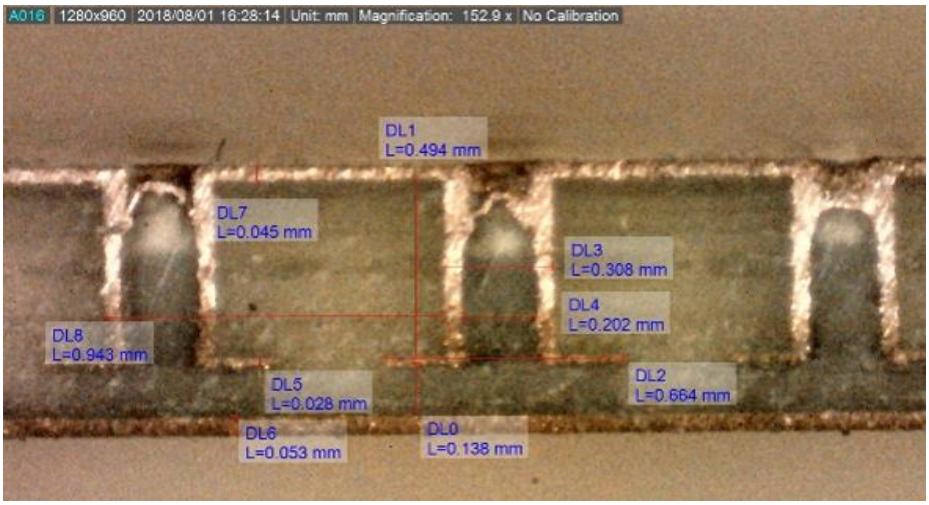

Figure 7. Micrographs showing the cross section X- X' of the fabricated PGGWG circuit

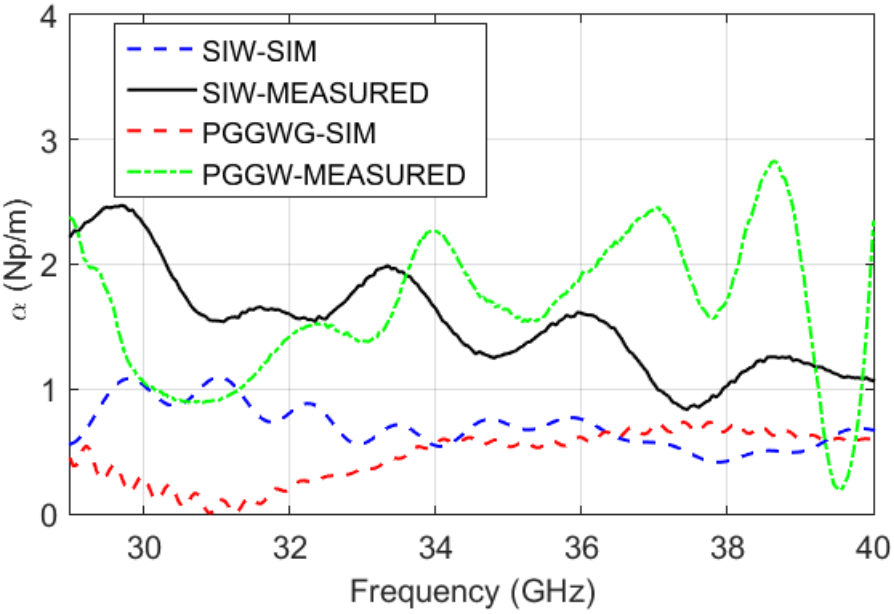

Figure 8. Attenuation constant (Np/m) of PGGWG and SIW

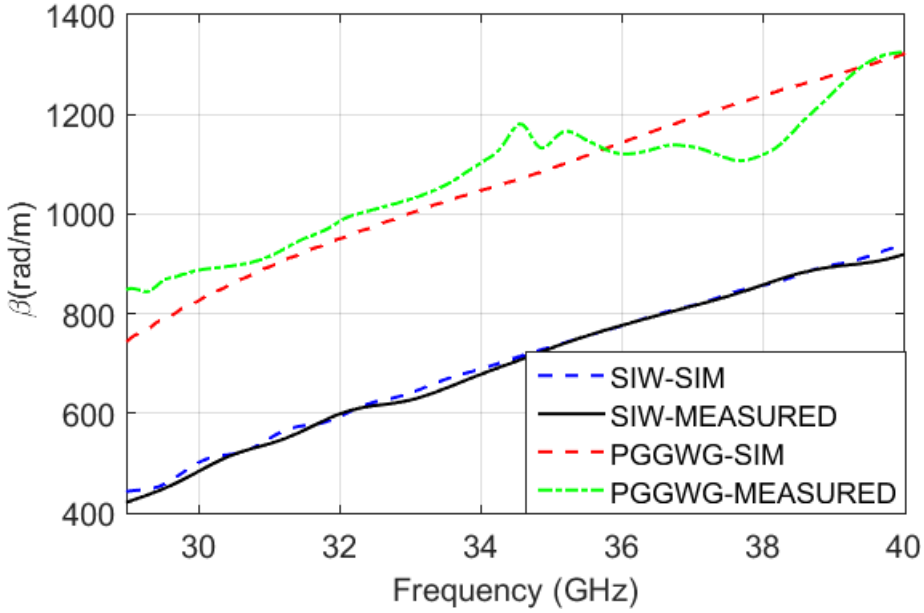

Figure 9. Phase constant (β/m) of PGGWG and SIW.

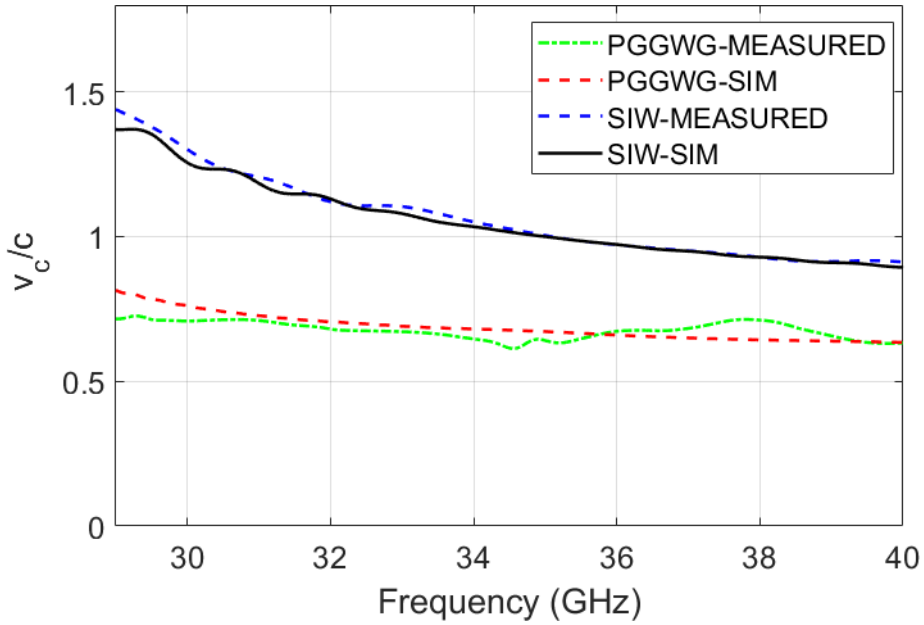

Figure 10. Phase velocity (v_c/c) of PGGWG and SIW

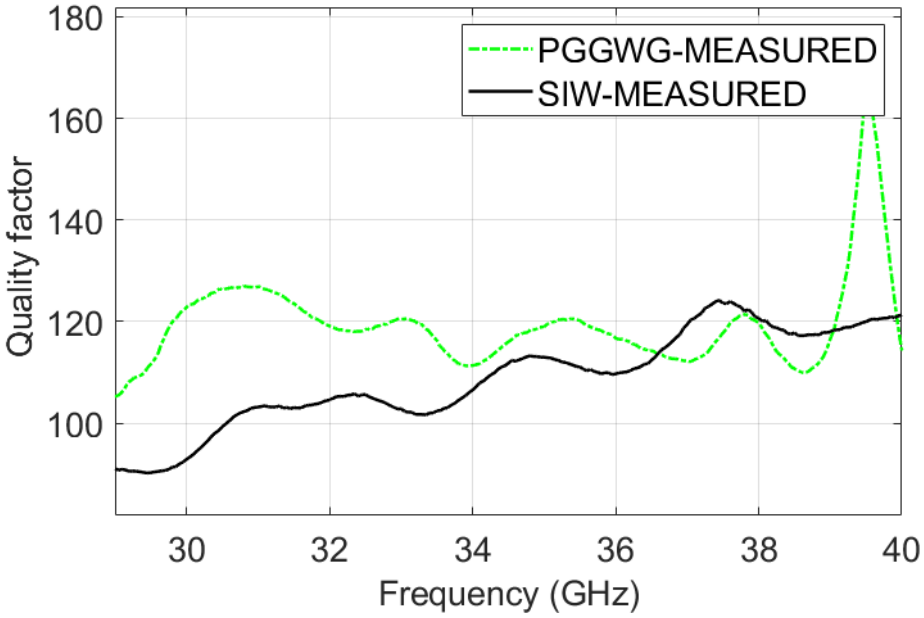

Figure 11. Transmission line Q-factor of PGGWG and comparable SIW.